Journal of Power Sources 212 (2012) 66–72

Contents lists available at SciVerse ScienceDirect

Journal of Power Sources

journal homepage: www.elsevier.com/locate/jpowsour

Applying functionalized carbon nanotubes to enhance electrochemical performances of tin oxide composite electrodes for Li-ion battery

Dongjoon Ahn [a,b], Xingcheng Xiao [a,*], Yawen Li [c], Anil. K. Sachdev [a], Hey Woong Park [d], Aiping Yu [d], Zhongwei Chen [d,**]

[a] Chemical Sciences and Materials Systems Lab, General Motors Global R&D Center, 30500 Mound Road, MC: 480-106-224, Warren, MI 48090-9055, USA
[b] Department of Chemical & Material Engineering, University of Kentucky, Lexington, KY 40506-0046, USA
[c] College of Engineering, Lawrence Technological University, Southfield, MI 48075, USA
[d] Department of Chemical Engineering, University of Waterloo, Waterloo, Ontario, Canada N2L3G1

ARTICLE INFO

Article history:
Received 3 February 2012
Received in revised form
14 March 2012
Accepted 16 March 2012
Available online 10 April 2012

Keywords:
Li-ion battery
Anode
Tin oxide
CNT

ABSTRACT

In this work, the tin oxide/carbon nanotubes (SnO_2/CNT) nanocomposite, where SnO_2 nanoparticles were deposited on the functionalized single wall CNTs, has been shown to exhibit desirable electrochemical performances as the negative electrodes for the lithium ion batteries. CNTs not only suppressed the mechanical degradation of SnO_2 and therefore provided the composite electrode with excellent capacity retention (>650 mAh g^{-1} with less than 10% capacity loss after 100 cycles), but also enhanced the electronic conductivity of the electrodes leading to excellent rate capability. The nanostructure of the nanocomposite has been shown to be critical for mitigating the mechanical degradation of electrodes.

1. Introduction

High energy and high power rechargeable Li-ion battery has become a key enabler for vehicle electrification including Plug-in Hybrid Electrical Vehicles and full Electric Vehicles (EV). Advanced electrode materials with further improved volumetric and gravimetric capacity are critical for further extend the driving range of those electric vehicles. Currently, graphite is the material widely used for the negative electrode in the Lithium Ion Batteries (LIBs) because of its good cycle performance and low cost. However, it has a relatively low theoretical capacity (372 mAh g^{-1}) and insufficient rate capability [1,2]. Many promising negative electrode materials have been explored in order to overcome those limitations; among them, SnO_2 is a potential candidate primarily due to its high capacity (790 mAh g^{-1}) [3]. However, the practical application of SnO_2 is limited by its poor cycling performance due to the large volume change (up to 250%) to the reduced Sn from SnO_2, which causes mechanical failure and loss of electrical contacts [4,5]. Also, the Li_2O formed from the first cycles might become the insulating matrix, leading to the increased impedance and poor rate capability.

Various synthesizing methods and techniques have been adopted in order to mitigate the mechanical degradation of SnO_2 electrodes. For example, SnO_2 nanowires [6,7] and nanotubes [8] were developed by several groups with different synthesis techniques and showed better cycle performance than SnO_2 powder. However, the high specific surface area of these nanomaterials could induce more side reactions such as forming large amount of Solid Electrolyte Interphase (SEI) layers [7,9], which instead increases the irreversible capacity loss of the electrode. Surface modification or coating is another effective method to improve the cycling stability because it can prevent the irreversible capacity loss by suppressing the side reactions.

However, since mechanical failure from the huge volume expansion is not effectively relieved by the thin coating covering the SnO_2, small scale architecture design, such as the fabrication of core-shell [10], hollow spheres [11,12] and nanotube arrays [13] are also an emerging technique to improve cycling stability of SnO_2. For instance, SnO_2 at carbon coaxial hollow spheres [12] have a stable capacity of about 500 mAh g^{-1} even after 200 cycles.

In this work, we applied the functionalized single wall CNTs as the buffering agent to suppress the mechanical degradation of SnO_2 based negative electrode and the conducting medium to facilitate

* Corresponding author. Tel.: +1 248 912 8132; fax: +1 586 986 9260.
** Corresponding author.
E-mail addresses: xingcheng.xiao@gm.com, xcxiao@gmail.com (X. Xiao), zhwchen@uwaterloo.ca (Z. Chen).

0378-7753/$ – see front matter © 2012 Elsevier B.V. All rights reserved.
doi:10.1016/j.jpowsour.2012.03.075

electron transport and lithium ion diffusion. We demonstrated that SnO_2/CNT based nanocomposite electrodes have significantly improved cycling stability and rate capability.

2. Experimental

The synthesis process of SnO_2-CNT is schematically shown in Fig. 1(a). Raw electric arc-discharge produced SWNTs with 30 wt% metal residue (Carbon Solutions, USA) was used as the starting material and as-received single walled CNTs were then refluxed in 16 M nitric acid for 1 h. The purpose of the nitric acid treatment was to remove the metal catalyst residue and to functionalize the CNTs with carboxylic acid groups [14,15].After cooling to room temperature, the black mixture was centrifuged at 3500 rpm for 15 min, after which the supernatant was decanted. The filtering process composed of (1) resuspension, (2) centrifugation and (3) decantation step, was repeated 4 times to remove the residue acid and amorphous carbon generated in the nitric acid treatment process. The resulting sediment was washed with deionized water to neutral pH and collected via membrane filtration. The single walled CNTs obtained were then purified and functionalized with carboxylic acid groups, which were called F-SWNTs.

To synthesize the SnO_2-SWNT support, tin precursor ($SnCl_2 \cdot 2H_2O$) was dissolved in 200 mL deionized water and mixed with 7 mL 38wt% HCl. SWNTs were dissolved in a separate beaker containing 200 mL deionized water and stirred until a good dispersion was achieved. The tin precursor solution was added to the mixture of CNTs at a relative ratio of $SnCl_2 \cdot 2H_2O$ to CNTs as 10: 1, after which the resulting mixture was homogenously dispersed for 30 min in an ultrasonic bath. After dispersing, the mixture was filtered and washed with deionized water again and dried overnight at 70 °C [16].

SnO_2/CNT composite electrodes composed of 80 wt% SnO_2/CNT composite, 10 wt% carbon black (Alfa Aesar, USA) and 10 wt% Polyvinylidene fluoride (PVDF, Alfa Aesar, USA), were used as the working electrode in a CR-2032 coin cell with lithium metal foil as both the reference and counter electrode. Microporous tri-layered polypropylene (PP) and polyethylene (PE) polymer membrane

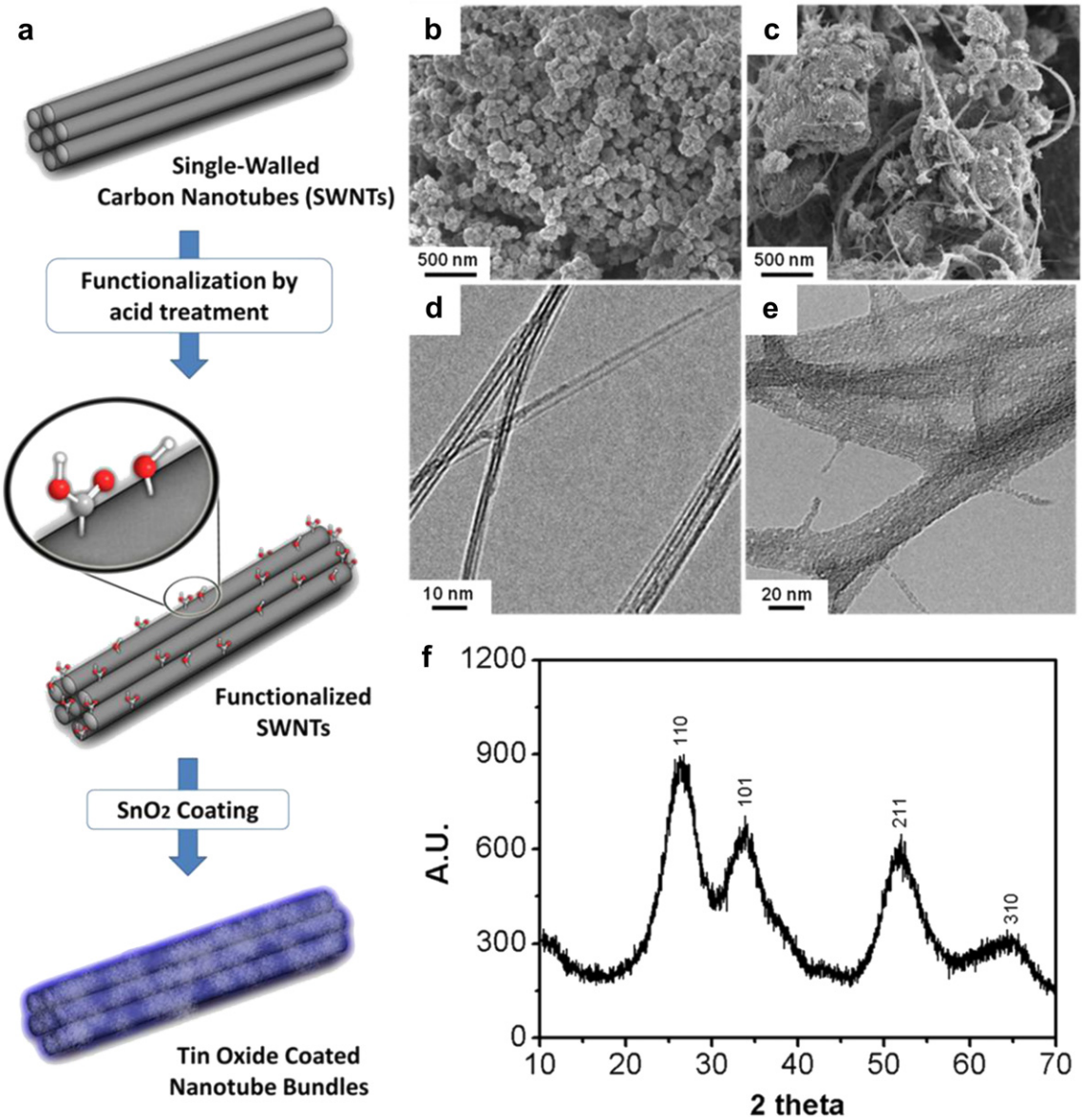

Fig. 1. (a) Schematic illustration of SnO_2/CNT composite developed from functionalized CNT, Scanning electron Microscopic images of (b) SnO_2 and (c) SnO_2/CNT powder, and Transmission electron Microscopy of (d) single walled CNT and (e) SnO_2/CNT composite and (f) XRD pattern for SnO_2/CNT composite.

(Celgard, USA) and 1 M $LiPF_6$ in a mixed solution of ethylene carbonate and diethyl carbonate (1:1 volume ratio, Novolyte, USA) were selected as the separator and electrolyte, respectively. The electrochemical measurements were performed at a constant current density of 25 mAg^{-1} at a cut-off voltage of 1 mV–2.5 V vs. Li/Li^+ to examine the capacity retention. For C-rate experiments, the current was increased by factor of two after every 10 cycles. Alternating Current (AC) impedance spectroscopy, using a sine wave with an amplitude of 10 mV over a frequency range from 1 mHz to 1 MHz, was applied to investigate the formation of the SEI layer and the charge transfer resistance of the SnO_2/CNT composite electrode under galvanostatic and potentiostatic conditions.

3. Results and discussion

Scanning Electron Microscopic (SEM) images of the SnO_2 powder and SnO_2/CNT composite are shown in Fig. 1(b) and (c), respectively. While the pristine SnO_2 in Fig. 1(b) are spherical to oval shaped sub-μm size particles, the SnO_2/CNT composite was an agglomerate of SnO_2 particles surrounded and connected by the CNT as shown in Fig. 1(c). Transmission Electron Microscopic (TEM) images of CNT as-received and SnO_2/CNT composite after completing the synthetic route are shown in Fig. 1(d) and (e), respectively. Overall, the tubular diameter of SnO_2/CNT composite was enlarged as a factor of 20 by SnO_2 deposition, in Fig. 1(e).

Fig. 1(f) presents X-ray diffraction (XRD) patterns of the CNT and SnO_2/CNT composite. All peaks from the XRD pattern of SnO_2/CNT correspond to a tetragonal SnO_2 phase. The main peaks of CNT(002) and SnO_2 (110) are almost superimposed [17], while the broad peaks of SnO_2/CNT are attributed to the poor crystallinity of SnO_2 due to the low synthesis temperature.

Fig. 2 shows the galvanostatic charge-discharge curve and differential capacity plots for investigating the effect of CNT on the electrochemical behavior of composite electrodes. Due to the mechanical fracture and electrical contact loss induced by volume expansion/contraction of SnO_2 upon cycling, the specific capacity of SnO_2 decreased continuously and became less than 200 mAh g^{-1} after the 3rd cycle, shown in Fig. 2(a). The electrochemical reaction mechanism for the SnO_2/Li cell was described as Eq. (1) and Eq. (2) [18,19];

$$SnO_2 + 4Li^+ + 4e^- \rightarrow 2Li_2O + Sn \quad (1)$$

$$Sn + xLi^+ + xe^- \leftrightarrow Li_xSn \ (0 \le x \le 4.4) \quad (2)$$

The first reaction from SnO_2 to Li_2O and Sn upon Li insertion, as shown in Eq. (1), was considered as the irreversible reaction because Li_2O is considered a very stable phase and the Li–O bond cannot break when Li is extracted. The second reaction, expressed in Eq. (2), indicates the reversible reaction while Li is inserted into

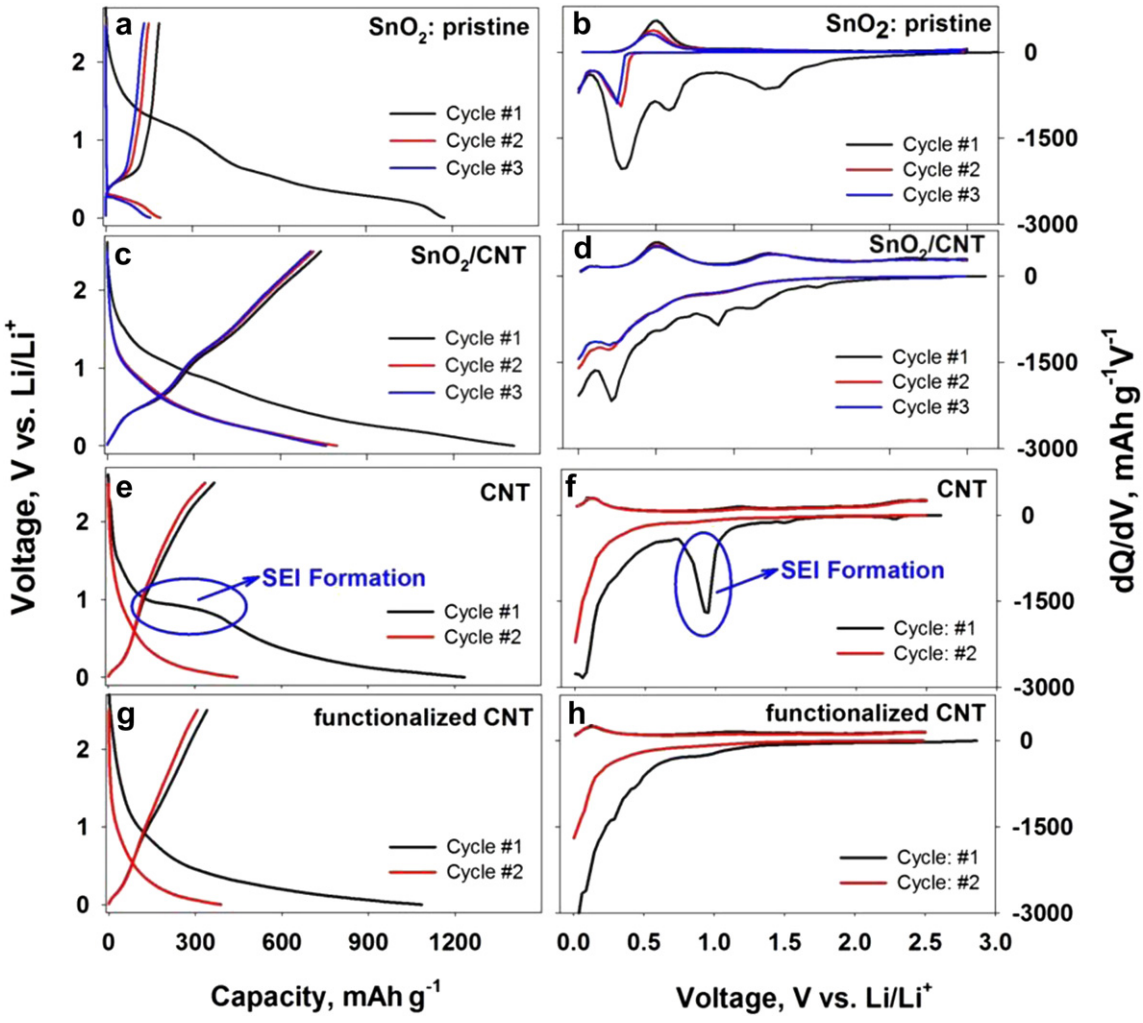

Fig. 2. Voltage profile and differential capacity plot of pristine SnO_2 (a & b), SnO_2/CNT composite (c & d) electrodes, pristine single wall CNTs (e & f) and functionalized CNTs (g & h).

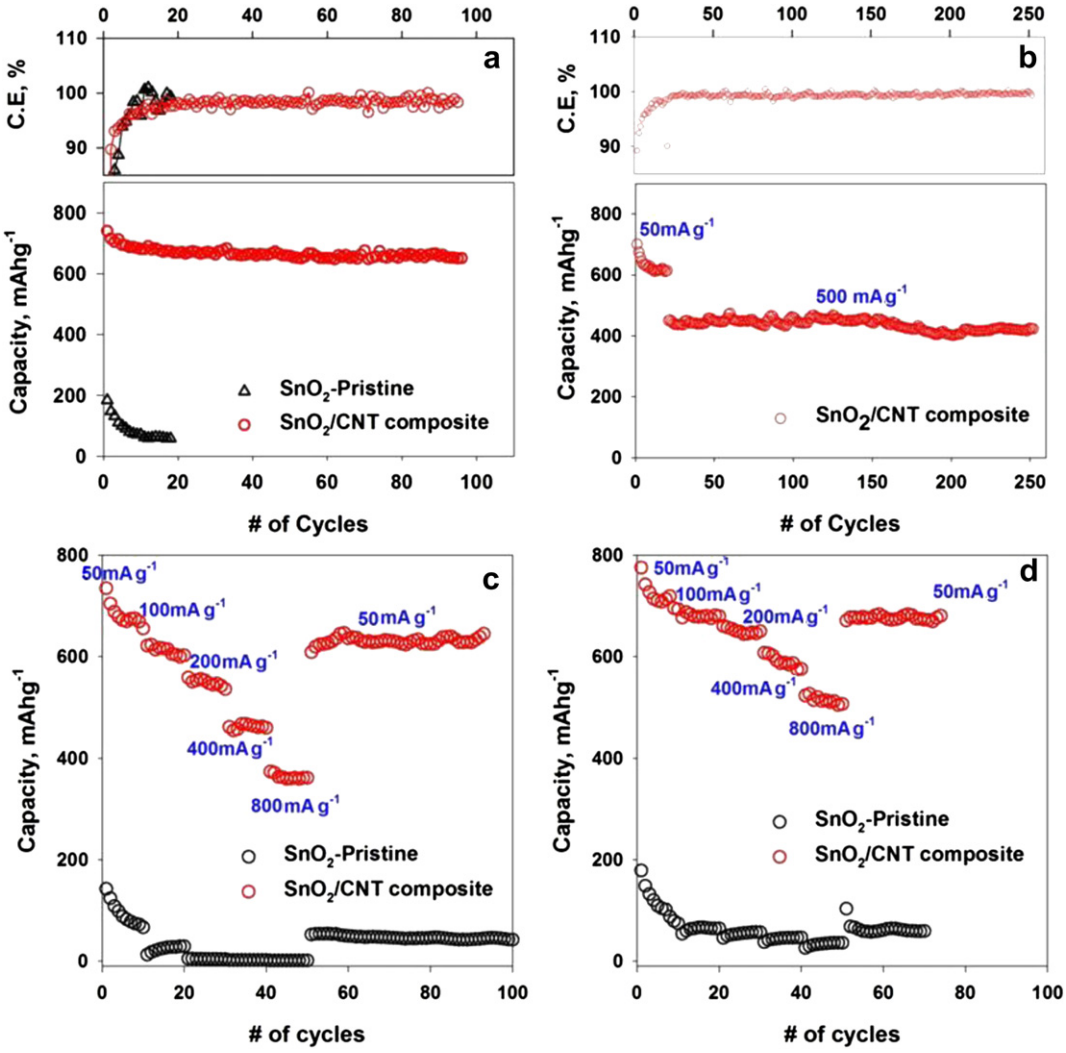

Fig. 3. Charge-discharge responses of pristine SnO_2 and SnO_2/CNT composite: (a) capacity retention & Coulombic efficiency under 25 mA g^{-1} current density, and C-rate capability of pristine SnO_2 (black circle) and SnO_2/CNT composite (red circle), (b) extended cycle performance & Coulombic efficiency of SnO_2/CNT composite with 50 mA g^{-1} and 500 mA g^{-1} current density, (c) symmetric charge-discharge cycles, and (d) asymmetric charge-discharge cycles. In symmetric cycles, both charge and discharge current density was doubled every 10 cycles. However, only charge current density was increased and discharge current density was set to 50 mAg^{-1} in the asymmetric cycles. (For interpretation of the references to color in this figure legend, the reader is referred to the web version of this article.)

and extracted from Sn. Due to the continuous insertion of Li into Sn, the Sn would form the $Li_{4.4}Sn$ phase [6].

In the case of pristine SnO_2, the reduction reaction from SnO_2 to Sn takes place in the first cycle and further lithium insertion into Sn generates an enormous volume change. When lithium was inserted and extracted continuously during many cycles, the lithium storage capacity became diminished due to the loss of electronic contact between Sn and the current collector as a result of mechanical degradation induced by the volume change. The differential capacity plot of the pristine SnO_2 in Fig. 2(b) showed three peaks corresponding to the reaction of SnO_2 to Sn (>1 V), SEI formation (0.9 V–0.5 V) and Sn to Li_xSn alloying (<0.5 V), respectively. Since the production of Li_2O and SEI formation are known as the irreversible reaction, the reaction corresponding to the alloying of lithium with Sn is only considered reversible for the subsequent lithium insertion cycle. The extraction of Sn from Li_xSn takes place at 0.4 V–0.7 V, and the peak intensity related to the capacity is reduced after several charge-discharge cycles due to the mechanical degradation of the Sn particle.

In contrast, the reversible capacity of SnO_2/CNT composite was around 750 mAh g^{-1}, with the first cycle irreversible capacity loss

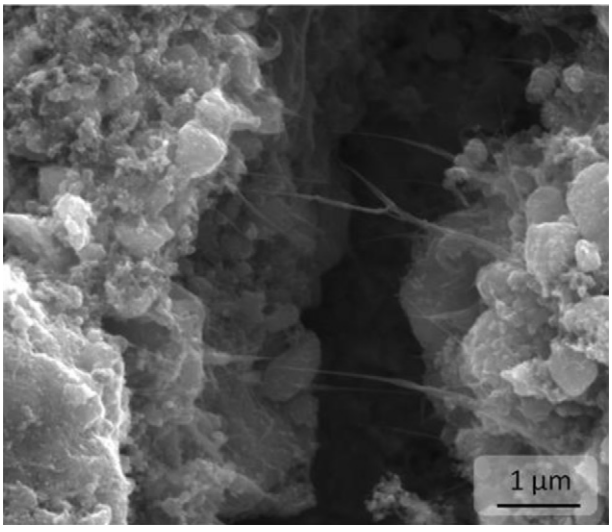

Fig. 4. Scanning electron Microscopic images of the SnO_2/CNT electrode.

around 650 mAh g^{-1} as shown in Fig. 2(c). The differential capacity plot of SnO_2/CNT composite in Fig. 2(d) showed two peaks during the charge cycle, and are referred to as de-alloying of LixSn to Sn (0.4 V–0.7 V) and de-intercalation of Li in Li-CNT (0.9 V–1.2 V) [20–22]. In the first charging cycle, the additional peaks are presented as a superposition with peaks from $Li_xSn \leftrightarrow Sn$ and $Li - CNT \leftrightarrow CNT$ reactions. The additional peaks are essentially the surface reaction of the boundary between electrolyte and the functionalized CNT. Also, the additional Li insertion behaviors such as a broaden peaks at 0.2 V–0.5 V was appeared in SnO_2/CNT composite compared to the pristine SnO_2 in Fig. 2(b) due to the lithium insertion into the single walled CNT in Ref. [2,23]. Based on the electrochemical behavior of single walled CNT from Claye *et al* [21], the irreversible capacity resulting from the CNTs in the composite is due to electrolyte reduction and formation of SEI on the carbon surface as evidence by the plateau at 0.9 V in the first discharge cycle. Consistent with their observation, we also observed an extended plateau in the voltage profile of pristine CNTs in Fig. 2(e) and a sharp peak in the differential capacity plot in Fig. 2(f), which is corresponding to the decomposition of the

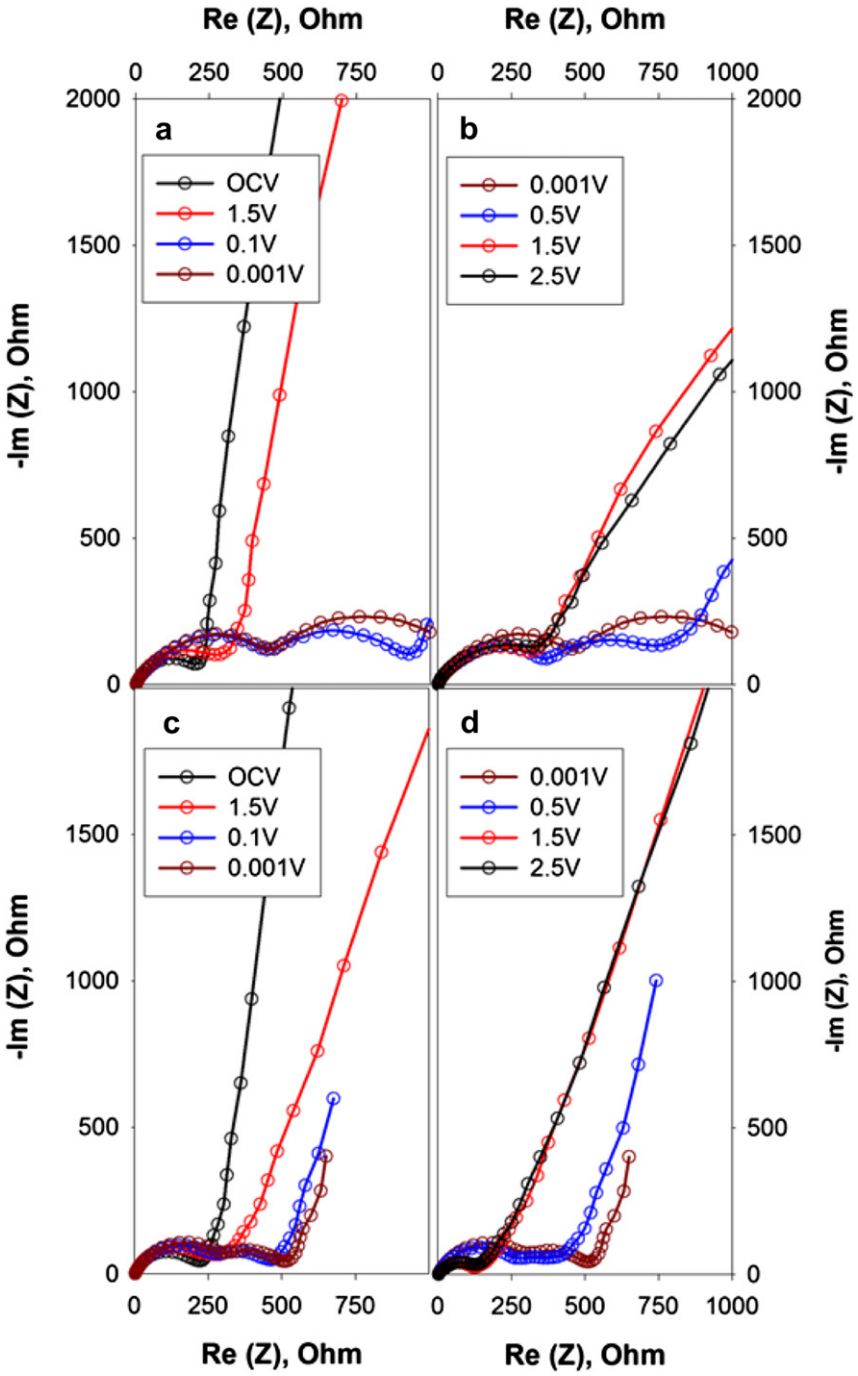

Fig. 5. Electrochemical impedance Spectroscopic (EIS) results of SnO_2 (a & b) and SnO_2/CNT composite (c & d) electrode with different state of charge (SOC) at 1st charging-discharging cycle.

electrolyte. In contrast, there is no such plateau and peak observed for functionalized CNTs in Fig. 2(g), which indicated that the carboxylic acid group presented on CNTs surface in fact suppress the electrolyte decomposition. We also believe that the carboxylic group helped the nucleation of SnO2 on CNT surface and enhanced the adhesion between them.

The charge capacity retention and Coulombic efficiency of the pristine SnO_2 and SnO_2/CNT composite are compared in Fig. 3(a). Similar to that shown in Fig. 2, the capacity retention of pristine SnO_2 was reduced from 200 mAh g^{-1} in the first cycle to less than 50 mAh g^{-1} after 10 cycles. For the SnO_2/CNT composite, the charge capacity was 750 mAh g^{-1} in the first charge cycle, although it decreased slightly during many charge-discharge cycles. Finally, the capacity of SnO_2/CNT composite was about 650 mAh g^{-1} after charging and discharging it 100 cycles, which is about 85% capacity retention compared to the first cycle. According to Fig. 3(a), the capacity degradation was not observed in the SnO_2/CNT composite, and it was mitigated by functionalizing the CNTs buffering fillers which inter-connect the Sn cluster [24]. It also shows that the SnO_2/CNT composite electrode has much better Coulombic efficiency than the pristine SnO_2 nanoparticles. In order to get more reliable data, longer capacity retention plot is shown in Fig. 3(b). During first 20 cycles, charging and discharging current density is applied as 50 mAg^{-1}, which is equivalent as C/14 rate, and then it increases 10 times higher than initial current density, which is equal to 1C rate, and continues to cycle more than 200 charging-discharging cycles. In spite of higher charging-discharging current and extended cycle number, the overall capacity has more than 60% of the initial capacity at low C-rate condition. Also, the capacity retention of SnO2/CNT composite is superior to any other commercial graphite electrode [25].

To investigate the C-rate capability of SnO_2/CNT composite, the specific capacity under different charge-discharge current density was measured and presented in Fig. 3(c). Both symmetric and asymmetric charge-discharge data are shown in Fig. 3(c) and Fig. 3(d), respectively. Similar to the capacity retention curve in Fig. 3(a) and Fig. 3(b), the specific capacity also slightly decreased, but stabilized after the 3rd or 4th cycle in the first 10 cycles for a current density of 50 mAg^{-1}. As the current density was increased from C/10 to 1C, the specific capacity reduced to 380 mAh g^{-1}, about half of its original specific capacity. In contrast, the specific capacity for natural graphite, the current negative electrode used in lithium ion battery, decreased about 10 times from 372 mAh g^{-1} down to 30 mAh g^{-1} when the cycling rate is increased from C/10 to 1C [26]. This indicates that the SnO_2/CNTs composite electrode has surprisingly good rate capability. On the other hand, under asymmetric charge-discharge conditions, the capacity at high C-rate is still around 500 mAh g^{-1}, indicating that this composite electrode could also have attractive power capability. When the current density was returned to the initial values of 50 mAg^{-1}, the specific capacity recovered to 600 mAh g^{-1}. There was no noticeable capacity fade even after another 50 cycles. For pristine SnO_2, however, the specific capacity was almost zero after the current density reached 200 mAg^{-1}. Fig. 4 shows the surface morphology of the SnO_2/CNT electrode after charging and discharging cycles was repeated 100 times. The CNTs clearly bridge the two agglomerates of SnO_2, and expectedly will enhance mechanical integration as well as electrical conductivity of the electrode during cycling.

Electrochemical Impedance Spectroscopic (EIS) measurements were carried out to confirm the effect of CNT on increasing the electronic conductivity in SnO_2/CNT composite electrodes. EIS results at seven different states of charge/discharge conditions are presented in Fig. 5. The *x*-axis intercept at high frequency was related to the overall cell resistance which was induced from the electrolyte, separator, and electrical contacts. The semi-circle of the high frequency impedance mainly presents the contact resistance between the composite electrode material and metallic current collector [27,28]. The other semi-circle at medium frequency is related to the lithium insertion resistance coupled with the capacitance of the interface between the active particles and the electrolyte. The overall impedances of the pristine SnO_2 electrode in Fig. 5(a) and (b) increased continuously through the entire cycle, while those for the SnO_2/CNT composite electrode did not change mainly because the CNT in the SnO_2/CNT composite increased the electrical conductivity. Additionally, the contact resistance in the pristine SnO_2 electrode increased due to the pulverization that occurred as a result of the volume change. For the composite electrode, the semi-circle related to the charge transfer resistance was reduced by almost one-half of its initial open circuit voltage when the SnO_2/CNT was charged back to over 1.5 V. It is believed that the lower impedance is due to the reduction reaction from SnO_2 to Sn as described in Eq. (2). Also, the reduced charge transfer resistance of SnO_2/CNT indicated that the electrical conductivity of SnO_2/CNT was enhanced due to the interconnection between SnO_2 particles by the functionalized CNTs.

4. Conclusions

In conclusion, a simple approach has been developed to synthesize SnO_2/CNT composites using functionalized CNTs without any subsequent heat treatment. SnO_2/CNT composite electrodes were shown to have a high specific capacity up to 650 mAh g^{-1} as well as stable cycling performance with 85% capacity retention after 100 cycles. Moreover, the C-rate capability was shown to be significantly improved by lowering the charge transfer resistance by the functionalized CNTs. We envision this material as a potential candidate for next generation negative electrode for high power and high energy Li-ion batteries.

Acknowledgments

The authors would like to thank Dr. Mark Verbrugge at GM R&D for helpful discussion. We acknowledge usage of the environmental scanning electron microscope at the Lawrence Technological University funded by the NSF MRI program (1040607).

References

[1] J.R. Dahn, T. Zheng, Y.H. Liu, J.S. Xue, Science 270 (1995) 590–593.
[2] J.M. Tarascon, M. Armand, Nature 414 (2001) 359–367.
[3] M. Armand, J.M. Tarascon, Nature 451 (2008) 652–657.
[4] I.A. Courtney, J.R. Dahn, J. Electrochem. Soc. 144 (1997) 2943–2948.
[5] D. Larcher, S. Beattie, M. Morcrette, K. Edstroem, J.C. Jumas, J.M. Tarascon, J. Mater. Chem. 17 (2007) 3759–3772.
[6] M.S. Park, G.X. Wang, Y.M. Kang, D. Wexler, S.X. Dou, H.K. Liu, Angew. Chem.-Int. Edit 46 (2007) 750–753.
[7] Y.D. Ko, J.G. Kang, J.G. Park, S. Lee, D.W. Kim, Nanotechnology 20 (2009) 6.
[8] Y. Wang, H.C. Zeng, J.Y. Lee, Adv. Mater. 18 (2006) 645–649.
[9] D. Larcher, C. Masquelier, D. Bonnin, Y. Chabre, V. Masson, J.B. Leriche, J.M. Tarascon, J. Electrochem. Soc. 150 (2003) A133–A139.
[10] H. Qiao, Z. Zheng, L.Z. Zhang, L.F. Xiao, J. Mater. Sci. 43 (2008) 2778–2784.
[11] X.W. Lou, D. Deng, J.Y. Lee, L.A. Archer, Chem. Mat. 20 (2008) 6562–6566.
[12] X.W. Lou, C.M. Li, L.A. Archer, Adv. Mater. 21 (2009) 2536–2539.
[13] A. Yu, E. Bekyrova, M.E. Itkis, D. Fakhrutdinov, R. Webster, R.C. Haddon, J. Am. Chem. Soc. 128 (2006) 9902–9908.
[14] H. Hu, A. Yu, E. Kim, B. Zhao, K.E. Itkis, E. Bekyarova, R.C. Haddon, J. Phys. Chem. B 109 (2005) 11520–11524.
[15] J.Z. Wang, N. Du, H. Zhang, J.X. Yu, D.R. Yang, J. Phys. Chem. C 115 (2011) 11302–11305.
[16] R.S. Hsu, D. Higgins, Z.W. Chen, Nanotechnology 21 (2010) 5.
[17] W.Q. Han, A. Zettl, Nano Lett. 3 (2003) 681–683.
[18] I.A. Courtney, J.R. Dahn, J. Electrochem. Soc. 144 (1997) 2045–2052.

[19] N. Li, C.R. Martin, J. Electrochem. Soc. 148 (2001) A164–A170.
[20] A. Dhanabalan, Y. Yu, X.F. Li, W. Chen, K. Bechtold, L. Gu, C.L. Wang, J. Mater. Res. 25 (2010) 1554–1560.
[21] F. Wang, G. Yao, M. Xu, M. Zhao, Z. Sun, X. Song, J. Alloy Comp. 509 (2011) 5969–5973.
[22] H.J. Wang, J.M. Wang, W.B. Fang, H. Wan, L. Liu, H.Q. Lian, H.B. Shao, W.X. Chen, J.Q. Zhang, C.N. Cao, Electrochem Comm. 12 (2010) 194–197.
[23] A.S. Claye, J.E. Fischer, C.B. Huffman, A.G. Rinzler, R.E. Smalley, J. Electrochem. Soc. 147 (2000) 2845–2852.
[24] T. Kim, Y.H. Mo, K.S. Nahm, S.M. Oh, J. Power Sourc. 162 (2006) 1275–1281.
[25] S.R. Sivakkumar, J.Y. Nerkar, A.G. Pandolfo, Electrochim. Acta 55 (2010) 3330–3335.
[26] J. Yi, X.P. Li, S.J. Hu, W.S. Li, L. Zhou, M.Q. Xu, J.F. Lei, L.S. Hao, J. Power Sourc. 196 (2011) 6670–6675.
[27] M. Gaberscek, J. Moskon, B. Erjavec, R. Dominko, J. Jamnik, Electrochem. Solid State Lett. 11 (2008) A170–A174.
[28] J.M. Atebamba, J. Moskon, S. Pejovnik, M. Gaberscek, J. Electrochem. Soc. 157 (2010) A1218–A1228.